Neuron
Article

Spike-Timing-Dependent Potentiation of Sensory Surround in the Somatosensory Cortex Is Facilitated by Deprivation-Mediated Disinhibition

Frédéric Gambino[1,2,*] and Anthony Holtmaat[1,2,*]
[1]Department of Basic Neurosciences, Faculty of Medicine
[2]Geneva Neuroscience Center
University of Geneva, CMU, 1 rue Michel Servet, 1211 Geneva, Switzerland
*Correspondence: frederic.gambino@unige.ch (F.G.), anthony.holtmaat@unige.ch (A.H.)
http://dx.doi.org/10.1016/j.neuron.2012.05.020

SUMMARY

Functional maps in the cerebral cortex reorganize in response to changes in experience, but the synaptic underpinnings remain uncertain. Here, we demonstrate that layer (L) 2/3 pyramidal cell synapses in mouse barrel cortex can be potentiated upon pairing of whisker-evoked postsynaptic potentials (PSPs) with action potentials (APs). This spike-timing-dependent long-term potentiation (STD-LTP) was only effective for PSPs evoked by deflections of a whisker in the neuron's receptive field center, and not its surround. Trimming of all except two whiskers rapidly opened the possibility to drive STD-LTP by the spared surround whisker. This facilitated STD-LTP was associated with a strong decrease in the surrounding whisker-evoked inhibitory conductance and partially occluded picrotoxin-mediated LTP facilitation. Taken together, our data demonstrate that sensory deprivation-mediated disinhibition facilitates STD-LTP from the sensory surround, which may promote correlation- and experience-dependent expansion of receptive fields.

INTRODUCTION

Sensory deprivation restructures cortical sensory maps, with active inputs gaining cortical space at the expense of less active ones (Merzenich et al., 1983). Some of the most compelling evidence for experience-dependent remodeling of adult cortical circuits has come from studies in the mouse primary somatosensory cortex (S1) (Feldman, 2009; Fox and Wong, 2005). "Barrel"-like clusters of cells in L4 of S1 have a strong one-to-one anatomical connection with the whiskers on the mouse's snout (Van der Loos and Woolsey, 1973). L4 cells project in a columnar fashion to supragranular pyramidal cells. As a result neurons in L2/3 have receptive fields that are strongly tuned toward one whisker, called the principal whisker (PW) (Figures 1A and 1B) (Armstrong-James et al., 1992). The nearest surrounding whiskers (SWs) constitute the periphery of the receptive fields. The removal of a subset of whiskers induces the input-deprived cortical cells to increase their subthreshold and suprathreshold responses to stimulation of the neighboring spared whiskers, causing the spared whisker representations to expand into the surrounding barrel columns (Diamond et al., 1994; Glazewski et al., 2000).

Multiple synaptic mechanisms have been proposed to drive the expansion of spared whisker representations in a partially deprived barrel cortex (Feldman, 2009). For example an imbalance in sensory input induces forms of synaptic long-term potentiation (LTP) that may strengthen latent intracortical connections (Clem and Barth, 2006; Finnerty et al., 1999; Glazewski et al., 2000), or stimulates the formation of new synapses whose stabilization may in turn depend on LTP-like processes (Cheetham et al., 2008; Hardingham et al., 2011; Wilbrecht et al., 2010). Tactile deprivation has also been shown to decrease the number of cortical inhibitory synapses (Chen et al., 2011; Keck et al., 2011; Micheva and Beaulieu, 1995) and reduce feedforward inhibitory currents in vitro (Chittajallu and Isaac, 2010; House et al., 2011; Jiao et al., 2006). Such disinhibition may allow sensory-driven excitation to spread over a larger population of supragranular pyramidal neurons (Kelly et al., 1999; Li et al., 2002) and to invade neighboring columns (Tremere et al., 2001). Despite strong evidence for each of these synaptic mechanisms separately, the interrelationship remains poorly studied in the context of barrel cortex plasticity.

Spike-timing-dependent plasticity (STDP), which is defined as the bidirectional modification of postsynaptic potentials (PSPs) after repeated coincidence of postsynaptic subthreshold and suprathreshold potentials (Markram et al., 1997), has been postulated as a Hebbian learning rule that could drive surround potentiation (Feldman, 2009; Sjöström et al., 2008). In acute slices of barrel cortex, the paired stimulation of L4-to-L2/3 inputs with back-propagating postsynaptic action potentials (APs) induces LTP in L2/3 neurons of the stimulated barrel column (Banerjee et al., 2009; Feldman, 2000; Hardingham et al., 2008) and in some occasions in the neighboring barrel column (Hardingham et al., 2011). Whisker deprivation rapidly changes the spike timing and spike order in barrel cortex (Celikel et al., 2004) and modulates the ability to induce spike-timing-dependent long-term potentiation (STD-LTP) in brain slices (Hardingham et al., 2008, 2011). Together, this suggests

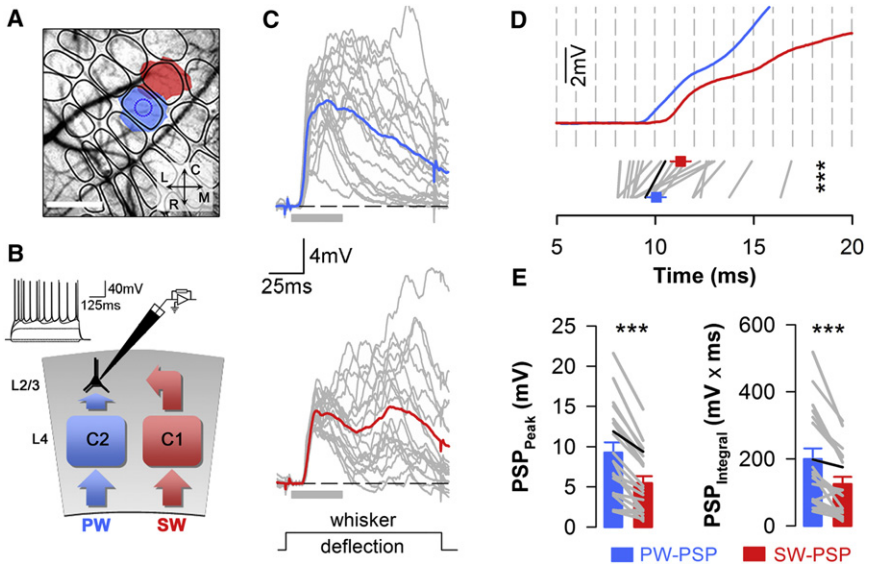

Figure 1. Recordings of Whisker-Evoked PSPs in L2/3 Cells in Vivo

(A) C2 (blue) and C1 (red) barrel-related columns were mapped using intrinsic optical imaging. L, lateral; C, caudal; R, rostral; M, medial. Scale bar, 500 μm.

(B) Patched L2/3 glutamatergic neurons in the C2 barrel column are characterized by regular spiking patterns.

(C) Average voltage responses of a single cell to PW (blue, C2) and to SW (red, C1) deflections are illustrated. Responses of 20 successive deflections are shown in gray. Gray box indicates extraction period for peak amplitudes and integrals.

(D) Onset latencies of PW- and SW-PSPs are presented. Onset stimulus artifacts are time locked to 0 ms.

(E) PSP peak amplitudes and PSP integrals are demonstrated.

Black lines in (D) and (E) represent examples in (C). Gray lines indicate paired experiments. ***$p < 0.001$, paired t test. Error bars, SEM.

See also Figure S1.

that barrel cortex map plasticity could be driven in vivo by a spike-timing-dependent mechanism, similar to retinal injury-induced visual cortex reorganization (Young et al., 2007). However, it is worth noting that most of the evidence for cortical STDP comes from studies in brain slices and that despite successful attempts to induce sensory input-mediated STD-LTP in the visual (Meliza and Dan, 2006) and auditory (Froemke et al., 2007) cortex, as well as STD long-term depression (LTD) in the somatosensory cortex (Jacob et al., 2007), whisker-evoked STD-LTP has not yet been demonstrated convincingly.

Here, we characterized whisker-evoked STD-LTP in vivo and investigated its effectiveness to drive surround potentiation in a model for experience-dependent cortical map plasticity, in which all except two neighboring whiskers are trimmed. It was previously shown that a brief period of this "dual-whisker experience" (DWE) causes the cortical representations of the two spared whiskers to overlap with one another (Diamond et al., 1994). We found that STD-LTP could be efficiently induced in the naive barrel cortex, but only by the PW and not by SW deflections. DWE induced a disinhibition of SW-evoked responses and facilitated surround STD-LTP.

RESULTS

STD-LTP Can Be Produced by PW but Not by SW Deflections

To study if STD-LTP could serve as a mechanism for sensory-driven response potentiation in the barrel cortex, we performed whole-cell recordings of supragranular pyramidal cells in vivo in one barrel column while repeatedly combining deflections of either the PW or SW with intracellular current injections. Prior to the whole-cell recordings, the C1 and C2 barrel columns were identified using intrinsic optical signal imaging (Figure 1A; see Figures S1A–S1C available online). Under anesthesia, regular spiking layer (L) 2/3 pyramidal cells in the C2 barrel column were blindly patched (Figure 1B). Consistent with previous findings, deflections of the PW (C2) or SW (C1) evoked compound PSPs with variable amplitudes (Brecht et al., 2003; Wilent and Contreras, 2004) (Figures 1C and S1D–S1K). To facilitate comparisons of PSPs under different conditions, further analysis was confined to the peak amplitudes and integrals within 40 ms after whisker deflection, and only if PSPs arose during membrane potential down states (for details see Experimental Procedures; Figures S1D–S1K). PW-evoked PSPs had slightly shorter onset latencies (PW, 10 ± 0.5 ms; SW, 11.3 ± 0.5 ms, $n = 20$; $p < 0.001$; Figure 1D), higher peak amplitudes (PW, 9.2 ± 1.3mV; SW, 5.4 ± 0.8mV, $n = 20$; $p < 0.001$; Figure 1E), and larger integrated potentials (PW, 199 ± 32mV×ms; SW, 124 ± 21mV×ms, $n = 20$; $p < 0.001$; Figure 1E) as compared to SW responses (Armstrong-James et al., 1992; Brecht et al., 2003).

To induce STD-LTP, we applied a classical AP-PSP-pairing protocol (Jacob et al., 2007; Markram et al., 1997). After a 5–10 min baseline recording, whisker-evoked PSPs were paired with suprathreshold current injections for 3–5 min (0.667 Hz). Current injections induced short AP bursts (2.7 ± 0.8 [SD] spikes/burst, $n = 54$; Figures 2A and S2A–S2C) and were timed in such a way that they followed the PSP onset. The spike-time delay was defined as the difference between the average latency of the first AP, as measured over the pairing period, and the average PSP onset latency, as measured over the baseline period (Δ delay; Figures 2A and S2A–S2C). We aimed at pairing both responses with Δ delays of less than 15 ms, which is a typical window for STD-LTP (Feldman, 2000; Markram et al., 1997). We analyzed the level of LTP as an average over the cell population as well as in individual cells. Pairing of PW-evoked PSPs with APs induced, on average, a long-lasting (24.1 ± 1.7 min) potentiation of subsequent PSPs (139% ± 6%, $n = 11$; $p < 0.001$; Figures 2B, 2D, and 2E). In contrast, pairing of SW-PSPs with APs failed to induce a potentiation (107% ± 2%, $n = 14$; $p > 0.1$; Figures 2C–2E). Similarly, the pairing procedure significantly enhanced the integrated PW-evoked PSPs,

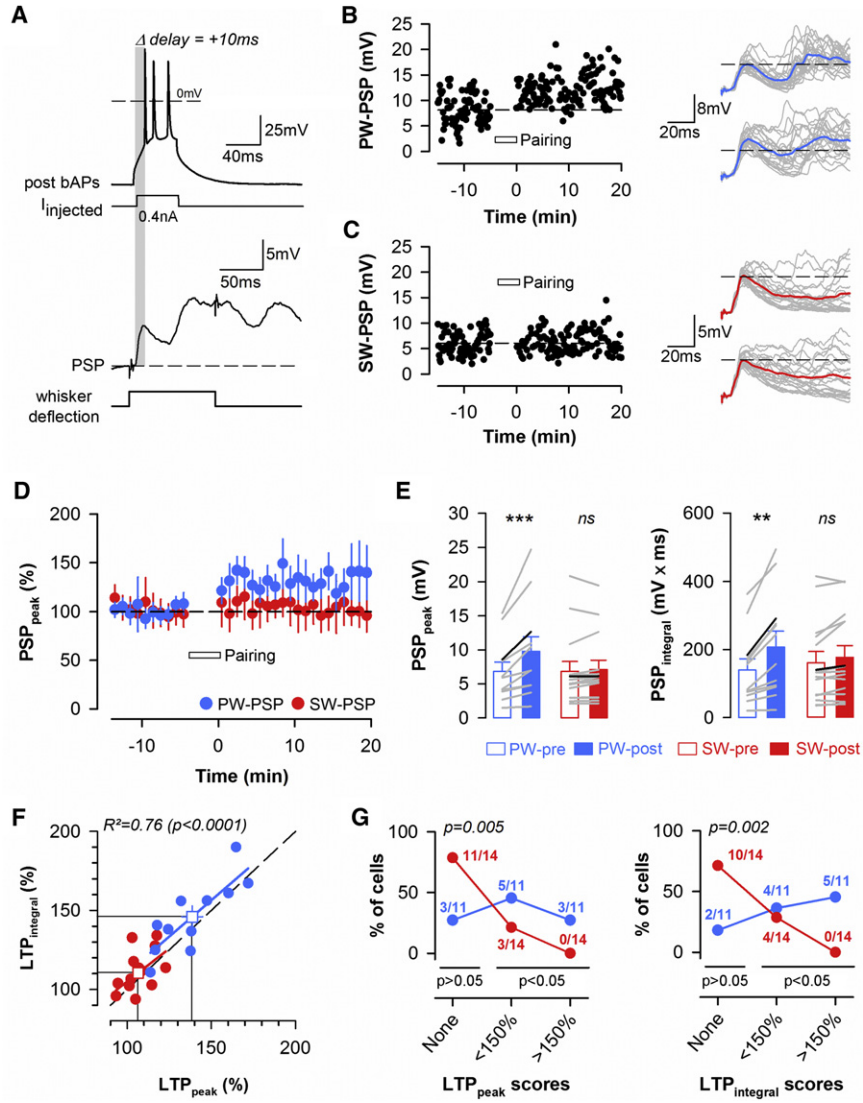

Figure 2. Induction of Whisker-Driven STD-LTP

(A) STD-LTP protocol is illustrated. Current injections ($I_{injected}$) induce back-propagating APs (post bAPs). Δ delay (gray bar) indicates the delay between the whisker-evoked PSP onset before the pairing (bottom panel) and the time of the first AP in the train during the pairing (top panel).

(B and C) Single-cell examples of STD-LTP induced by pairing PW (B) or SW (C) PSPs with bAPs are presented. Left panels demonstrate PSP peak amplitudes over time. Right panels show individual trials (gray) and average membrane potentials (bold lines) before (top) and after (bottom) the pairing. Dashed lines indicate mean PSP peak amplitude before the pairing.

(D) Time course of mean PW- and SW-PSP amplitudes (±SEM) after STD-LTP induction is illustrated. Only cells paired with Δ delays <15 ms were averaged.

(E) Mean PSP peak amplitudes and PSP integrals (±SEM) are presented. Gray lines indicate pairs. Black lines represent examples in (B) and (C). ns, not significant. $^{**}p < 0.01$, $^{***}p < 0.001$, paired t tests.

(F) Relationship between the LTP levels based on PSP peak amplitudes and PSP integrals is demonstrated. Error bars, SD.

(G) Results of a two-sided Kolmogorov-Smirnov test for cells displaying no LTP ("None," $p > 0.05$) or significant LTP ($p < 0.05$) based on PSP peak amplitudes and PSP integrals are shown. Cells displaying significant LTP are further categorized according the level of LTP ("<150%" or ">150%" of baseline). The proportions of cells expressing moderate-to-high levels of SW-driven LTP display a negative linear trend, significantly different from the PW (Cochran-Armitage test for trend).

See also Figure S2.

whereas it failed to change the integrated SW-evoked responses (Figures 2E and 2F). The level of LTP based on PSP integrals was linearly related to the level of LTP based on PSP peak amplitudes. This indicates that LTP could reliably be detected using both parameters and that it was largely absent for the SW (Figure 2F). Whereas PW-evoked PSP-AP pairing induced significant LTP ($p < 0.05$, Kolmogorov-Smirnov test), ranging from moderate to high levels in 8 (PSP peak) or 9 (PSP integral) out of 11 cells, SW-PSP-AP pairing induced significant and moderate levels of LTP in only 3 (PSP peak) or 4 (PSP integral) out of 14 cells, and completely failed to potentiate responses in the other cells (Figure 2G). Thus, significantly more cells tended to express higher levels of LTP upon PW deflections, as compared to SW deflections (Figure 2G). Together, these data indicate that in contrast to PW-evoked PSPs, SW inputs to L2/3 pyramidal cells are not reliably potentiated using a classical STDP protocol.

PW-Driven STD-LTP Depends on Postsynaptic Mechanisms

We characterized the main requirements for the induction of STD-LTP. In agreement with in vitro studies by Feldman (2000), PW-driven LTP could not be elicited when we intentionally used Δ delays longer than 15 ms (30.8 ± 9 ms, n = 4; Figures 3A–3C). Under these conditions the mean PW-evoked PSP amplitude remained similar to the baseline (102% ± 8%, n = 4; $p > 0.1$; Figure 3C). LTP was neither induced when PSPs were not paired with APs (100% ± 5%, n = 6; $p > 0.1$).

Prolonged cell dialysis (33 ± 7 [SD] min after break-in, n = 3) also prevented PW-driven LTP (103 ± 0.8, n = 3; $p > 0.1$; Figure 3F), suggesting that it was dependent on postsynaptic induction or expression mechanisms. To determine whether an increase in postsynaptic Ca^{2+} concentration through NMDA receptors (NMDARs) was required for STD-LTP, we included the NMDAR open-channel blocker MK-801 (1 mM, n = 5) in the recording pipette solution (Humeau et al., 2005). MK-801 efficiently prevented the induction of PW-driven LTP (Figures 3D–3F). Together, this indicates that the mechanisms for

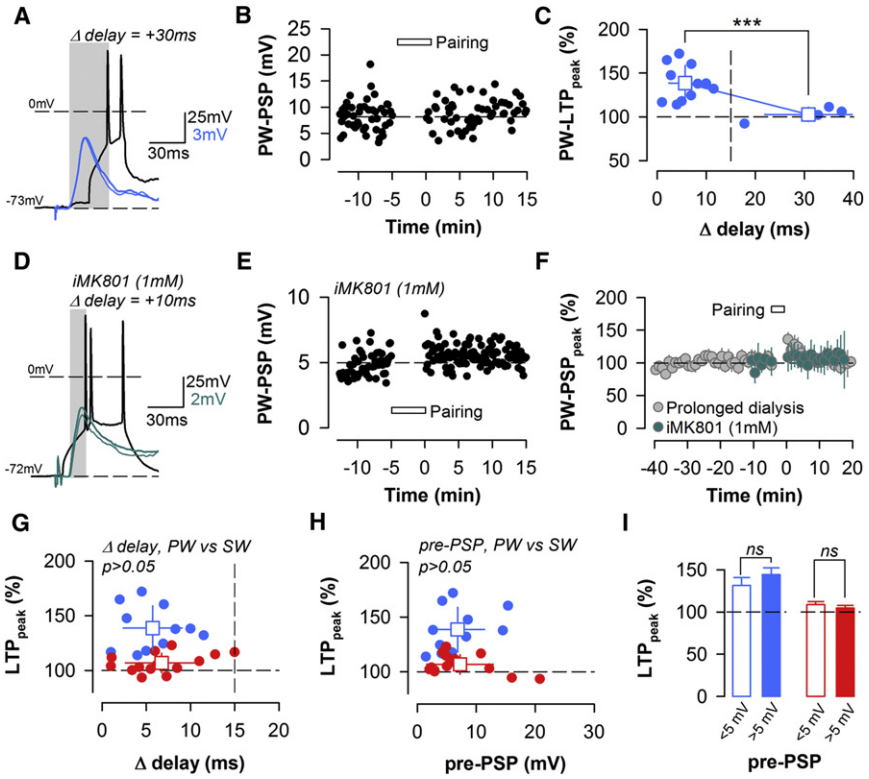

Figure 3. Characterization and Comparison of PW- and SW-Driven STD-LTP

(A) Example of an STD-LTP experiment with Δ delays >30 ms is illustrated.

(B) PSP amplitudes before and after pairing are presented.

(C) The percentage of potentiation as a function of Δ delay is demonstrated. Circles indicate cells; squares represent averages for Δ delays <15 and >15 ms. ***p < 0.001, unpaired t test. Error bars, SD.

(D) Example of an STD-LTP experiment after intracellular dialysis of MK-801 (iMK801, 1 mM) is shown.

(E) PSP amplitudes before and after pairing are illustrated.

(F) Mean PSP peak amplitudes (±SEM) before and after pairing with iMK801 (cyan) and during prolonged recording dialysis (gray) are presented.

(G and H) The percentage of potentiation as a function Δ delays (G) and the averaged baseline PSP amplitudes prior to STD-LTP induction (pre-EPSP; H) are demonstrated. Circles indicate individual cells; squares represent averages. PWs are in blue; SWs are in red. p Values are calculated by an unpaired t test. Error bars, SD.

(I) Levels of LTP categorized by low (<5mV) and high (>5mV) pre-PSP values (±SEM) are shown. ns, not significant; unpaired t test.

See also Figure S2.

PW-driven LTP were congruent with postsynaptic STDP (Feldman, 2000; Jacob et al., 2007; Markram et al., 1997; Sjöström et al., 2008).

STDP Parameters Are Similar between the PW and SW

To exclude the possibility that different success rates between PW- and SW-driven LTP were based on coincidental differences in the STDP protocol, we compared its key parameters. The average Δ delays that were used in the pairing protocols did not differ between the PW and SW (PW, Δ delay = 5.7 ± 1 ms, n = 11; SW, Δ delay = 6.7 ± 1 ms, n = 14; p > 0.1; Figure 3G), indicating that the lower success rates of SW-driven STD-LTP could not be accounted for by differences in PSP and AP latencies. In the LTP experiments the baseline SW-evoked PSP amplitudes were similar to the baseline PW-evoked PSP amplitudes (PW-pre-EPSP, 6.8 ± 1.3mV, n = 11; SW-pre-EPSP, 7.2 ± 1.5mV, n = 14; p > 0.9), and we could not detect a correlation between the average baseline whisker-evoked PSP amplitudes and the subsequent levels of LTP (PW, r^2 = 0.14, p = 0.256; SW, r^2 = 0.18, p = 0.13; Figures 3H and 3I). Neither did the PSP increase correlate with the pairing duration, the total number of APs, the mean number of APs per burst, the interspike intervals, or the AP frequency (Figure S2C). No statistical differences in these parameters were detected between the PW and SW (Figure S2C). Because PSP-AP pairings may be more efficient in up states than in down states, we confirmed that pairing had occurred equally frequent in both states for the PW and SW. PW-driven LTP was somewhat lower but still significant when analyzed regardless of up or down states, and the absence of SW-driven LTP could not be explained by the restriction of our analysis to down states (Figures S2D–S2G). Together, these comparisons indicate that the lack of SW-driven LTP was not likely caused by variations in baseline values, analysis criteria, or STDP protocol parameters.

DWE Facilitates SW-Driven LTP

The nonpermissive nature of the SW-associated synaptic pathway to STD-LTP is at odds with studies that have linked LTP and STDP-like mechanisms to whisker deprivation-induced surround response potentiation (Clem and Barth, 2006; Diamond et al., 1994; Feldman, 2009; Glazewski et al., 2000). We reasoned that whisker deprivation might induce a form of metaplasticity in L2/3 cells that allows spared whisker-driven STD-LTP, facilitating the response to surround whisker deflections. To test this hypothesis, we exposed mice to a brief period (2.4 ± 0.9 [SD] days, n = 28) of DWE by clipping all except the C1 and C2 whiskers (Figure 4A). In this model surround potentiation has been suggested to involve STDP (Diamond et al., 1994; Feldman, 2009).

DWE did not significantly change the mean PW- and SW-evoked PSP peak amplitudes (PW, 9.3 ± 1.4mV, n = 20, p = 0.9; SW, 7.7 ± 1.1mV, n = 20, p = 0.121; compare Figures 4B and 1E), or PSP integrals (PW, 235 ± 32mV×ms, n = 20, p = 0.337; SW, 188 ± 25mV×ms, n = 20, p = 0.055; compare Figures 4C and 1E) as compared to normal whisker experience. Although SW-evoked PSPs were still smaller than PW-evoked PSPs (peak, p < 0.01; integral, p < 0.01; Figures 4B and 4C), the ratio of the SW-/PW-evoked PSP amplitudes (SW/PW control, 0.58 ± 0.04; SW/PW DWE, 0.82 ± 0.06; p < 0.01; Figure 4D)

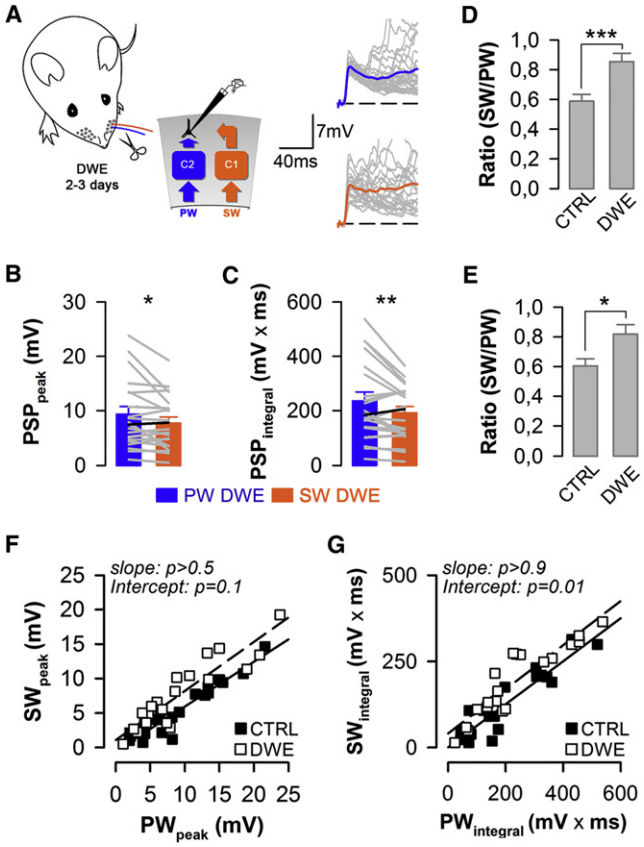

Figure 4. Whisker-Evoked PSPs after DWE

(A) Left panel shows all except two neighboring whiskers (C1 and C2) are trimmed (DWE). Right panels are single-cell averages (20 traces) of PW (blue)- and SW (orange)-PSPs in DWE mice.

(B and C) Average PW- and SW-PSP peak amplitudes (B) and PSP integrals (C) (±SEM) are illustrated. *p < 0.05, **p < 0.01, paired t test. Gray lines indicate paired experiments. Black line represents example in (A).

(D and E) SW/PW ratio of PSP peak amplitudes (D) and PSP integrals (E) (±SEM) in control (CTRL) and deprived (DWE) mice is presented. *p < 0.05, ***p < 0.001, t tests.

(F and G) Relation between SW- and PW-PSP peak amplitudes (F) and PSP integrals (G) in control (CTRL, open square) and deprived (DWE, filled square) mice is demonstrated. Lines indicate linear regression fits. The intercepts in (G) were statistically different between CTRL and DWE (p = 0.01, ANCOVA).

and integrals (SW/PW control, 0.64 ± 0.03; SW/PW DWE, 0.84 ± 0.04; p < 0.05; Figure 4E) had significantly increased upon DWE. Therefore, although DWE had not potentiated PW- or SW-associated synaptic inputs at the population level, SW-associated inputs had gained relative strength in individual cells. Interestingly, this increase was evident for cells with high as well as low PSP integrals, indicating that DWE had affected SW-associated inputs of strongly as well as weakly connected cells (Figures 4F and 4G). We verified whether the slightly enhanced SW-evoked PSP amplitudes had caused an increase in SW-evoked spiking, as was previously observed in this model by Diamond et al. (1994) (data not shown). In control mice the PW elicited on average 0.04 ± 0.11 spikes per deflection (n = 33 cells), whereas the SW elicited only 0.02 ± 0.05 (n = 33 cells), which is in the same range as previous findings by Brecht et al. (2003). DWE had not changed PW-evoked spiking (0.05 ± 0.16, n = 26 cells), whereas the SW-evoked spiking rates had tripled (0.07 ± 0.15; n = 34 cells). When the analysis was restricted to spiking cells only, this increase proved to be significant (p < 0.001). Together, these data demonstrate that DWE subtly changes SW-evoked PSP amplitudes and thereby increases average SW-evoked spiking rates.

We next tested whether DWE had increased the susceptibility for STD-LTP. Similar to the control conditions, the pairing of PW-evoked PSPs with APs readily induced LTP (142% ± 13%, n = 7; p < 0.05; Figures 5A, 5C, and 5D). The average level of LTP was not significantly different from controls (Figure 5E). Interestingly, the pairing of SW-evoked PSPs with APs now also induced LTP (127% ± 6%, n = 8; p = 0.002; Figures 5B–5D). The average level of SW-driven LTP was significantly higher as compared to controls (Figure 5E) and similar to PW-driven LTP (p = 0.305). This could not be explained by a change in postsynaptic excitability (Figures S3A and S3B). The increase in SW-driven STD-LTP was evident in both peak PSP amplitudes and PSP integrals (Figure 5C). The fraction of cells that displayed significant levels of SW-driven LTP had increased (p = 0.014) and now followed a trend that approached the PW-driven LTP scores (p = 0.479; Figure 5F). Both the average Δ delays in the paring protocol and the baseline SW-evoked PSP amplitudes did not differ between controls and DWE animals (Figures S3C and S3D). In general the baseline PSP amplitude was not correlated with the success rate of LTP induction (Figures S3E–S3H), indicating that the increase in SW-driven LTP upon DWE was not due to a relative change in baseline SW-evoked excitatory synaptic responses. Similarly, although the variability in the SW-evoked PSP onset delays had become similar to the PW-evoked responses, this was not significantly correlated to the success rate of LTP induction in our data set (Figures S3I–S3K).

DWE Is Associated with a Reduction in SW-Evoked Inhibitory Input

What could be the mechanism underlying the facilitation of SW-evoked STD-LTP upon DWE? Sensory deprivation has been shown to reduce feedforward inhibition in vitro (Chittajallu and Isaac, 2010; House et al., 2011; Jiao et al., 2006), and a blockade of inhibition was shown to facilitate tetanic stimulation-mediated LTP in the barrel cortex (Glazewski et al., 1998). We hypothesized that DWE might also suppress SW-evoked inhibitory responses and thereby enhance the susceptibility of this synaptic pathway to STD-LTP.

We measured whisker-evoked excitatory and inhibitory conductances as well as the latencies of the excitatory and inhibitory synaptic current onsets using voltage-clamp recordings. Recordings were made at various holding potentials (Vh = −100–0mV) to generate synaptic current-voltage (I–V) curves for every cell (Figures 6A and 6B). A cesium-based internal solution containing QX-314 was used to block potassium, sodium, and GABA-B-R conductances (Monier et al., 2008). Only recordings with an initial series resistance (Rs) lower than 40 MΩ (mean, 25 ± 8 MΩ [SD], n = 21) and a Rin/Rs ratio higher than 3 (mean, 7.1 ± 4 [SD], n = 21) were analyzed (Figures S4A and S4B). This allowed us to compare cells under various conditions (see

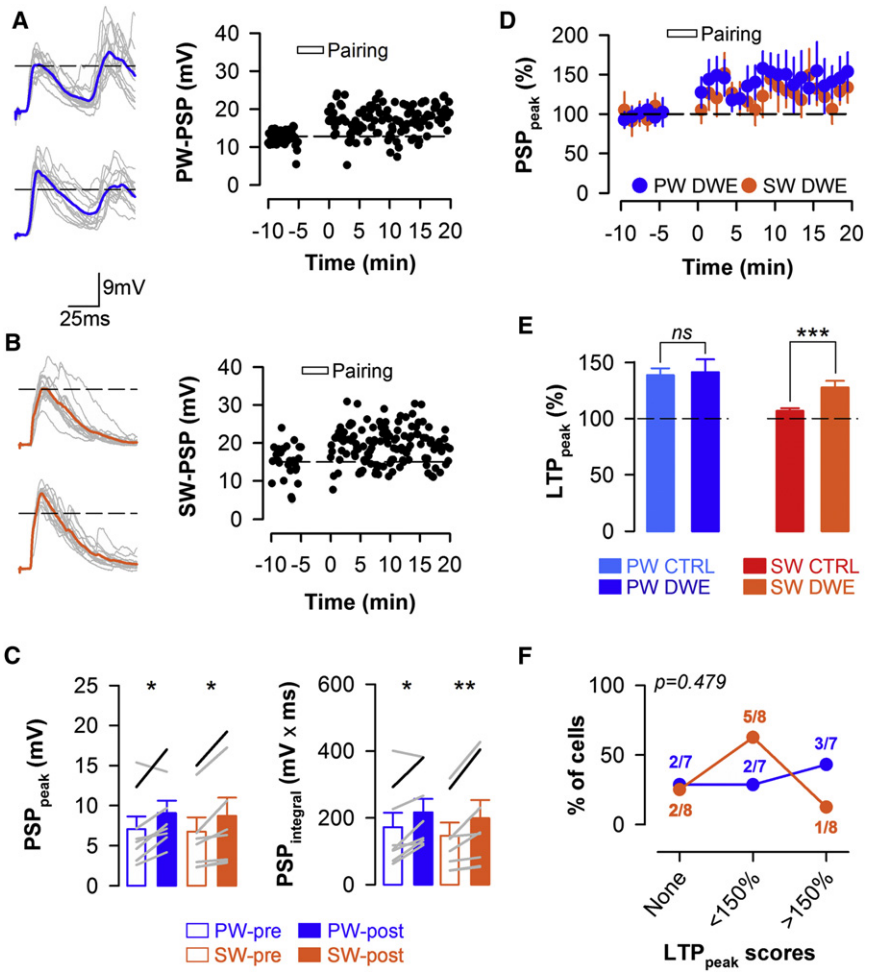

Figure 5. DWE Facilitates SW-Driven STD-LTP

(A and B) Single-cell examples of STD-LTP induced by pairing of PW (A) or SW (B) PSPs with bAPs after DWE are illustrated. Left panels show individual trials (gray) and average membrane potentials (bold) before (top) and after (bottom) the pairing. Dashed lines indicate mean PSP peak amplitude before the pairing. Right panels present PSP peak amplitudes over time.

(C) Mean PSP peak amplitudes and PSP integrals (±SEM) before and after the pairing are demonstrated. Gray lines indicate pairs. Black lines represent examples in (A) and (B). *$p < 0.05$, **$p < 0.01$, paired t tests.

(D) Time course of average PW- and SW-PSP peak amplitudes (±SEM) normalized to baseline after DWE is illustrated.

(E) Mean of PW- and SW-PSP peak amplitudes (±SEM) normalized to baseline, in controls and after DWE, is shown. ***$p < 0.001$, pairwise multiple comparisons (Dunn's method, $\alpha = 0.05$) after nonparametric Kruskal-Wallis one-way ANOVA on ranks ($p < 0.001$); CTRL: PW, n = 11, SW, n = 14; DWE: PW, n = 7, SW, n = 8.

(F) After DWE, the proportions of cells expressing moderate-to-high levels of SW-driven LTP display a similar trend to PW-driven LTP (Cochran-Armitage test for trend).

See also Figure S3.

Experimental Procedures). Under all conditions we found linear relationships between the integrated currents over a 5- to 40-ms-poststimulus period and the Rs-corrected holding potentials (Vcs) (R^2, control PW: 0.96 ± 0.02 [SD], n = 14; control SW: 0.95 ± 0.03 [SD], n = 17; DWE PW: 0.95 ± 0.04, n = 11; DWE SW: 0.95 ± 0.05, n = 12) (Figure 6B). This indicates that NMDAR conductances had not or only minimally contributed to the responses (Manookin et al., 2008; Monier et al., 2008). Based on the I–V regression slopes and the synaptic reversal potentials, we calculated the inhibitory (Gi) and excitatory (Ge) conductances over time (Figures 6B–6F) (House et al., 2011; Monier et al., 2008). Inhibitory (Ei) and excitatory (Ee) reversal potentials were estimated to be −100 and 0mV, respectively. Calculation of Ei was based on an estimated extracellular chloride concentration ($[Cl^-]_e$) of 180 mM, which we verified pharmacologically in a subset of the recordings (Supplemental Experimental Procedures; Figures S4C–S4G). The similarity between the derived and calculated reversal potentials indicates that the voltage clamps were rather accurate and that the calculated Gi and Ge were not greatly affected by a limited space clamp (Supplemental Experimental Procedures). Integrated conductances over a 40 ms period were used as a measure of the total Ge and Gi (Figures 6C–6F).

Compared to control conditions, DWE had not significantly changed PW-evoked Ge and Gi (Ge: control, 153 ± 30 nS.ms; DWE, 157 ± 32; $p > 0.9$; Gi: control, 137 ± 31 nS.ms; DWE, 122 ± 25 nS.ms; $p > 0.9$) (Figures 6C and 6E). However, whereas DWE had left the SW-evoked Ge largely unchanged, it had reduced the SW-evoked Gi by more than 50% (Ge: control, 79 ± 12 nS.ms; DWE, 57 ± 11 nS.ms; $p = 0.2$; Gi: control, 79 ± 11 nS.ms; DWE, 37 ± 8 nS.ms; $p < 0.01$) (Figures 6D and 6F). The notion that the SW- and not the PW-mediated Gi had decreased on the same neurons indicates that DWE had mostly influenced the SW-associated pathway and that these effects were very unlikely to be accounted for by space-clamp limitations (see Experimental Procedures). Because our estimated Ei was lower than the values that are classically reported for recordings in vitro, we recalculated the Gi and Ge over a range of Ei values: −60mV ($[Cl^-]_e$ = 40 mM) to −110mV ($[Cl^-]_e$ = 250 mM). Under all assumed Ei values, DWE had significantly lowered the SW-mediated Gi, whereas PW-evoked conductances were unaffected (Figures S4H–S4K). This indicates that the decrease in inhibition was robust.

In a complete deprivation paradigm, the decrease and delay in inhibitory conductance in vitro are compensated by a decrease and delay in excitatory conductance to maintain the Gi:Ge ratio and timing constant (House et al., 2011). In our DWE model the deprivation-mediated decrease in SW-evoked Gi was also accompanied by a small decrease in Ge, but this was insignificant and failed to rebalance SW-evoked Gi:Ge ratios

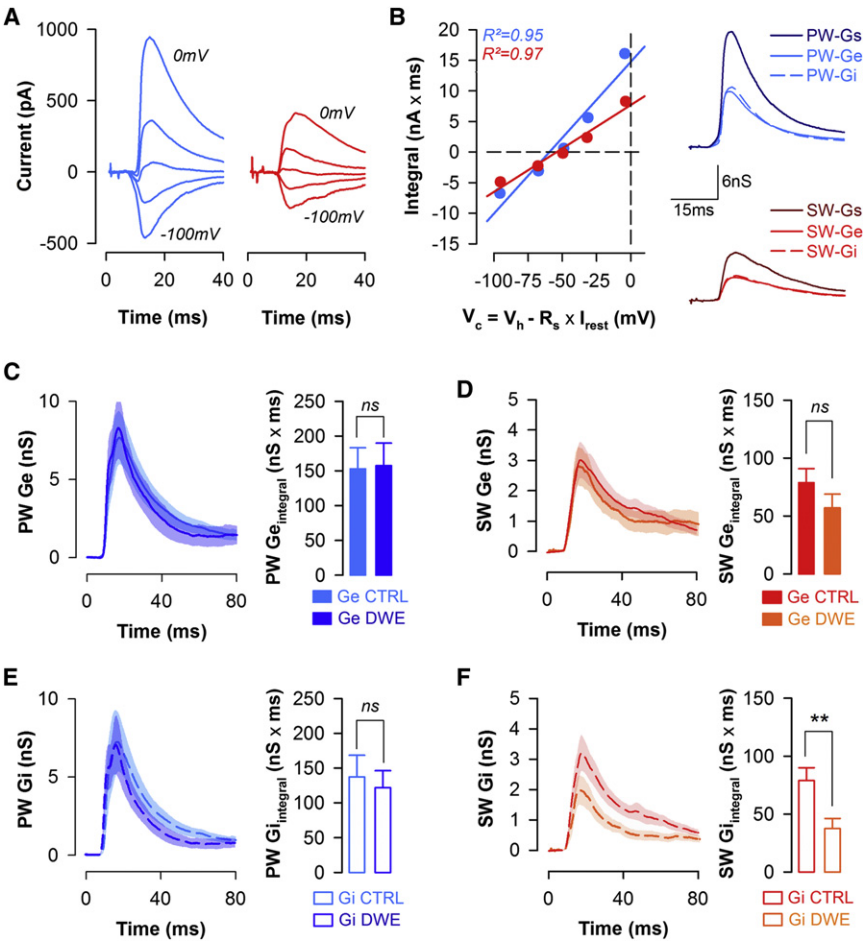

Figure 6. DWE Mediates Changes in SW-Evoked Inhibitory Conductances

(A) Examples of PW (blue)- or SW (red)-evoked average currents, taken from one cell that was clamped at five different holding potentials.

(B) Left panel is synaptic IV curves for the examples in (A). Integrated currents plotted against the Vcs are presented. Linearity is assessed for each recorded cell by linear regression. Right panel is synaptic conductance (Gs) over time for the examples in (A) and (B).

(C–F) Left panels show averaged PW (C and E)- and SW (D and F)-evoked synaptic excitatory (C and D) and inhibitory (E and F) conductances over time in controls and after DWE. Shaded areas indicate SEM. Right panels illustrate mean integrated conductance (±SEM). **p < 0.01, t tests (PW, CTRL, n = 14, DWE, n = 11; SW, CTRL, n = 17, DWE, n = 12).

See also Figure S4.

(Figures 6D and 7A). As a result the fraction of inhibition was significantly lower for SW-evoked responses after DWE (Gi/(Ge+Gi), control, 0.51 ± 0.01, n = 14; DWE, 0.37 ± 0.03, n = 13; p < 0.001; Figure 7B). Under control conditions the PW-evoked inhibitory postsynaptic current (IPSC) onsets recorded at Vh = 0mV always followed the PW-evoked excitatory postsynaptic current (EPSC) recorded at Vh = −100mV (Figures 7C and 7D). In contrast, SW-evoked IPSCs preceded on average the PW-evoked EPSCs ($t_{IPSC} - t_{EPSC}$, PW, 1.1 ± 0.2 ms; SW, −0.4 ± 0.3 ms; p < 0.001; Figures 7C and 7D). After DWE the relative latencies of the SW-evoked IPSCs had changed. The average difference in the latencies between IPSCs and EPSCs ($t_{IPSC} - t_{EPSC}$) was now positive for the SW (SW, 0.14 ± 0.32 ms, n = 13; Figure 7D), and although it had not significantly changed as compared to controls, it had become almost similar to the latency differences that were observed for the PW (Figure 7E). Together, these data indicate that DWE disproportionately attenuates the SW-associated inhibitory inputs on L2/3 pyramidal cells.

Blocking of Inhibition Facilitates SW-Driven STD-LTP

The concurrent reduction in SW-evoked inhibition and facilitation of SW-driven STD-LTP after DWE suggests that the disinhibition is a permissive factor for STD-LTP. We tested whether a block of L2/3-GABA-A-Rs by PTX could also facilitate SW-driven LTP. To avoid generalized epileptic activity of cortical networks, we applied PTX to the intracellular recording solution, which likely results in small and local diffusion of the drug in and around the recorded neuron (Figure 8A). Whisker-evoked outward currents were nearly absent at 0mV, indicating that PTX had successfully blocked GABA-A-Rs (Figures S4C and S4D). In contrast to the control conditions, SW-evoked PSPs could be readily potentiated upon pairing with APs (Figures 8B–8D) under PTX. Postpairing PSP peak amplitudes were now significantly higher than baseline PSPs (pre, 8.9 ± 1.6mV; post, 14.7 ± 2.3mV; p < 0.001; Figure 8D), and the level of LTP was significant (171% ± 11%; p < 0.001; Figure 8E). The fraction of cells that displayed significant LTP was also higher than under control conditions (p = 0.027; Figure 8F). This suggests that a reduction of the inhibitory drive facilitates STD-LTP.

DWE Partly Occludes PTX-Mediated Facilitation of STD-LTP

To test whether the observed facilitation of SW-driven STD-LTP after DWE was indeed connected to reduced inhibition, we also measured the PTX-mediated increase in SW-driven LTP after DWE. We hypothesized that if PTX allows similar levels of SW-evoked LTP after DWE as compared to controls, the facilitating effect of PTX would be partly occluded, and disinhibition may have indeed been an important facilitating factor. On the other hand, if PTX allows higher levels of SW-evoked LTP, the facilitating effect of PTX would not be occluded, and additional mechanisms of metaplasticity may have instead played a dominant role in the facilitation of LTP.

Similar as in control mice, PTX facilitated the induction of SW-driven LTP after DWE (Figure 8C). Postpairing PSP amplitudes

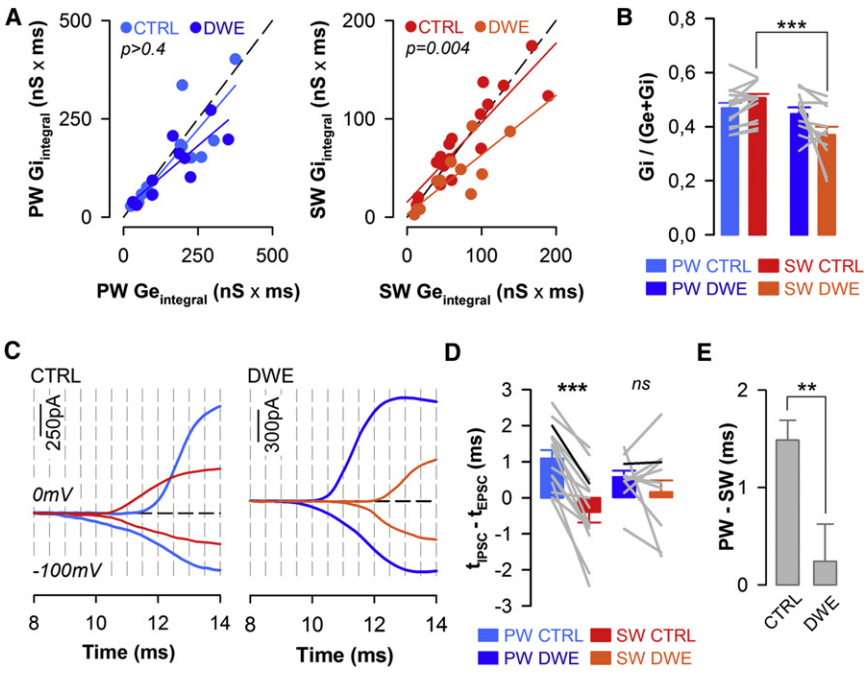

Figure 7. DWE Causes a Fractional Increase and Delay in SW-Evoked Inhibition

(A) Relation between integrated Ge and Gi for PW and SW, in controls and after DWE, is demonstrated. Colored solid lines indicate linear regression fits. Dashed line represents identity line. Slopes of the linear regressions were statistically different for the SW (ANCOVA).

(B) The excitatory/inhibitory ratio (Ge/(Ge+Gi)) (±SEM) based on the integrated Ge and Gi is illustrated. The ratio is significantly higher for the SW after DWE as compared to the SW in control mice. ***$p < 0.001$, pairwise multiple comparisons (Dunn's method, $\alpha = 0.05$) after Kruskal-Wallis one-way ANOVA on ranks ($p < 0.001$). Gray lines indicate paired experiments.

(C) Average traces at Vh = −100 and 0mV upon PW and SW deflections, in controls and after DWE, are shown.

(D) Difference between the mean onset of inhibition and excitation ($t_{IPSC} - t_{EPSC}$) (±SEM) for PW and SW currents is presented. ***$p < 0.001$, paired t test. Gray lines indicate paired experiments. Black line represents example from (C).

(E) Difference between the mean PW and SW current delays (($t_{PW\text{-}IPSC} - t_{PW\text{-}EPSC}$) − ($t_{SW\text{-}IPSC} - t_{SW\text{-}EPSC}$)) (±SEM) in controls and after DWE is demonstrated. **$p < 0.01$, t test (CTRL, n = 15; DWE, n = 11).

were significantly higher than baseline PSPs (pre, 7.2 ± 2.5mV; post, 11.4 ± 3mV, n = 5; $p < 0.05$; Figure 8D), and the fraction of cells with significant LTP scores had increased (Figure 8F). However, PTX-mediated levels of LTP did not exceed the levels that were observed under control conditions (CTRL+iPTX, 171% ± 11%, n = 8; DWE+iPTX, 167% ± 15%, n = 5; p = 0.815; Figure 8E). Thus, the fractional increase in the level of LTP due to PTX was lower after DWE than in controls (control, +60%; DWE, +30%), indicating that the DWE-mediated reduction in inhibition had partly occluded the PTX-mediated facilitation of STD-LTP. Altogether, this suggests that the DWE-mediated disinhibition of the SW-associated synaptic pathway had been responsible for the facilitation of SW-driven STD-LTP.

DISCUSSION

We showed that pairing of PW-evoked PSPs with injected APs induces LTP in L2/3 pyramidal cells of the barrel cortex in vivo. LTP induction was only successful in pairings with less than a 15 ms PSP-AP latency (i.e., "pre-leading-post") and depended on postsynaptic NMDARs (Figures 2 and 3). Together, this suggests that LTP induction followed the requirements for STDP (Markram et al., 1997; Sjöström et al., 2008), in line with studies in barrel cortex in vitro (Feldman, 2000; Hardingham et al., 2003) and other sensory systems in vivo (Froemke et al., 2007; Meliza and Dan, 2006). Our findings complement a previous study in which a "post-leading-pre" STDP protocol efficiently induced synaptic depression in vivo (Jacob et al., 2007). In that same study STD-LTP was also produced in a low number of cells, but not as robustly and efficiently as in our study. There are several differences between the studies that could have caused this, such as the number of paired stimuli, pairing delay times, analysis criteria, species, and age (Banerjee et al., 2009). Furthermore, we used intrinsic-optical signal mapping to locate the PW-associated barrel column (Figure S1), whereas the previous study identified the PW based on the "best" response from a group of neighboring whiskers. The latter method may not preclude selection of cells near the border of a neighboring column (Sato et al., 2007). Thus, we may have selected a more homogeneous population of cells within the confines of the PW-associated barrel column that more consistently responded to the STD-LTP protocol.

We found that STD-LTP could not readily be produced when SW-evoked PSPs were paired with APs (Figure 2). This was unexpected because in accordance with previous studies (e.g., Brecht et al., 2003), the SW evoked significant subthreshold PSPs (Figure 1). Moreover, in our STDP experiments the pairing parameters as well as the PSP amplitudes were indistinguishable between the PW and SW (Figures 3 and S2) and were, therefore, unlikely to be accountable for the failure to induce significant SW-driven LTP. A lack of LTP could also be due to deficiencies in the molecular machinery that mediates it (e.g., NMDARs, CaMKII, and PKA levels). However, our finding that SW-evoked PSPs could be potentiated after a GABA-A-R block (Figure 8) suggests that the post- and presynaptic plasticity machinery is present in the SW-associated pathway (Hardingham et al., 2008). Nevertheless, our data are consistent with previous studies, in which direct tetanic stimulation of L4-to-L2/3 synapses in vivo (Glazewski et al., 1998), or STDP protocols ex vivo, poorly induced LTP across barrel columns of naive mice (Hardingham et al., 2011). Together, this suggests that

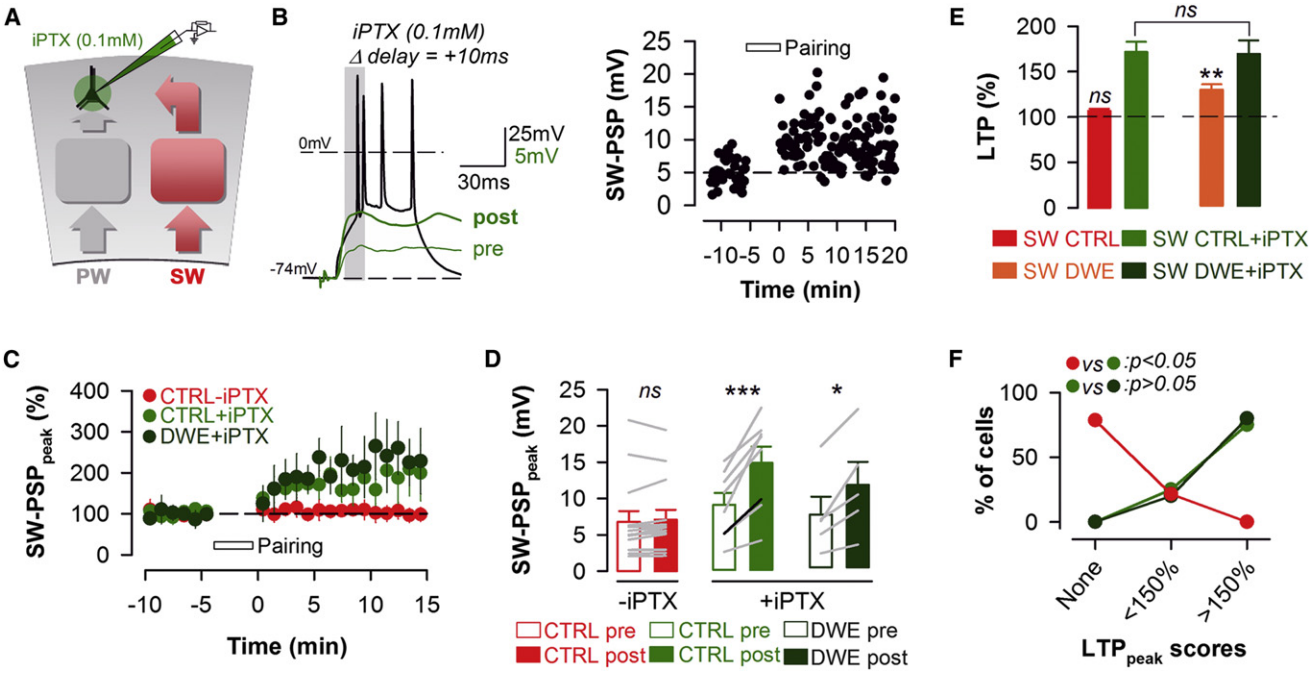

Figure 8. Pharmacological- and Deprivation-Mediated Disinhibition Facilitates SW-Driven STD-LTP

(A) PTX was applied to the intracellular recording solution (iPTX, 0.1 mM), which likely diffuses (green area). SW-evoked responses were recorded.

(B) Example of an STD-LTP experiment with iPTX is illustrated. Left panel shows PSP amplitudes before (pre) and after (post) pairing of bAPs and SW-PSPs. Right panel presents time course of PSP amplitudes.

(C) Time course of average SW-PSP peak amplitudes (±SEM) normalized to baseline in the absence (−iPTX) or presence of PTX (+iPTX), in controls and after DWE, is shown.

(D) Mean SW-PSP peak amplitudes (±SEM) before and after the pairing, in controls and after DWE, are presented. Gray lines indicate pairs. *$p < 0.05$, ***$p < 0.001$, paired t tests (CTRL-iPTX, n = 14; CTRL+iPTX, n = 8; DWE+iPTX, n = 5).

(E) Mean SW-PSP peak amplitudes (±SEM) normalized to baseline, in the presence or absence of PTX, in controls and after DWE are demonstrated. **$p < 0.01$, paired t tests; NS, not significant, pairwise multiple comparisons (Dunn's method, $\alpha = 0.05$) after Kruskal-Wallis one-way ANOVA on ranks ($p < 0.001$).

(F) Under iPTX the proportions of cells expressing moderate-to-high levels of SW-driven LTP follow the same trend in control and deprived mice (Cochran-Armitage test for trend).

under normal circumstances PW-evoked PSPs may be potentiated, but SW-evoked PSPs are unlikely to be potentiated, upon increased concomitant postsynaptic and presynaptic spiking.

Our finding that pairing of PW-evoked PSPs with APs efficiently produced LTP supports the notion that LTP may underlie experience-dependent PW-driven response potentiation during normal development of the barrel cortex (Takahashi et al., 2003) and after single whisker experience (SWE) (Clem and Barth, 2006). Whisking behavior may induce neuronal firing rates and PSP-spike-time delays that are supportive of STD-LTP of PW responses (Celikel et al., 2004; Kimura et al., 2010), which may serve as a mechanism to strengthen and tune L2/3 receptive fields (Komai et al., 2006). Continued susceptibility of PW-evoked responses to STD-LTP in adulthood may function to increase sensitivity to PW-related inputs during learning. The low probability to induce surround STD-LTP on the other hand may prevent SWs from gaining excessive synaptic input during normal whisking and to maintain receptive field tuning in an intact system. Indeed, in the adult barrel cortex, receptive fields only modestly overlap in supragranular layers, do not readily change, and may even sharpen upon sensory enrichment (Feldman, 2009; Polley et al., 2004).

Difference in Susceptibility of PW and SW Inputs to STD-LTP

What are the characteristics of the PW- and SW-associated synaptic pathways that could render them differently susceptible to STD-LTP? The most obvious distinction is that part of the PW-evoked responses is transmitted through intracolumnar L4-to-L2/3 projections onto basal dendrites, whereas the SW-evoked activity first ascends to L2/3 of a neighboring barrel column and then spreads into transcolumnar horizontal L2/3-to-L2/3 projections that are intertwined with both basal and apical dendrites (Figure 1B) (Lübke and Feldmeyer, 2007; Petersen et al., 2003). Thus, the PW may activate a fractionally higher number of synapses on proximal dendrites as compared to the SW (Lübke and Feldmeyer, 2007; Petreanu et al., 2009). For L2/3 pyramidal neurons of the visual cortex, it has been shown that STDP tends to induce lower levels of LTP in distal dendritic inputs (Froemke et al., 2005). This is possibly due to a strong attenuation of back-propagating APs toward distal dendrites (Sjöström et al., 2008), resulting in lower NMDAR activation levels in apical as compared to basal dendrites. In the barrel cortex such a mechanism could render SW-associated synapses less sensitive to STDP. Differences in clustering or

functionality of synapses may also cause contrasting levels of plasticity (Humeau et al., 2005), but it is as yet unclear if such differences exist between PW- and SW-associated inputs (Varga et al., 2011).

Lateral or vertical forward inhibition (Adesnik and Scanziani, 2010; Chittajallu and Isaac, 2010; House et al., 2011; Kimura et al., 2010; Swadlow and Gusev, 2002) could further sculpt the differences between PW- and SW-associated excitatory pathways. In our study the inhibitory/excitatory conductance ratio was slightly but significantly higher for SW-evoked responses as compared to PW-evoked responses (Figures 6 and 7). In addition the inhibitory currents preceded on average the excitatory currents for the SW, whereas for the PW the inhibitory currents occurred after excitation. This prompts the speculation that the SW recruits a different or an additional and slightly more potent inhibitory circuit, which may efficiently constrain the temporal summation of EPSPs (Pouille and Scanziani, 2001) or shunt back-propagating APs (Tsubokawa and Ross, 1996) and contribute to the insensitivity to forms of plasticity. In support of this we found that a block of GABAergic inputs greatly facilitated SW-driven STD-LTP (Figure 8). Altogether, it is likely that differences in both excitatory and inhibitory pathways render the SW-associated inputs less permissive to STD-LTP than the PW-associated synapses.

Facilitation of Surround STD-LTP after Deprivation

We showed that trimming of all except two neighboring whiskers facilitated the induction of SW-driven STD-LTP (Figure 5). This is in line with an ex vivo study in which across-barrel STD-LTP was facilitated after deprivation (Hardingham et al., 2011). Whisker trimming did not change the baseline levels of SW- and PW-evoked responses at the population level. However, the average SW/PW ratio had increased for most cells (Figure 4). Because the recorded neurons were current clamped above the inhibitory reversal potential (Ei = −100mV), this could have been caused by a reduction in SW-associated inhibition (Kelly et al., 1999). Alternatively, excitatory synapses from surround inputs could have been potentiated (Glazewski et al., 2000). Interestingly, DWE did not block or occlude STD-LTP for either the PW or SW. This suggests that if LTP was expressed at this stage, it had not yet saturated whisker-response potentiation. This is different from observations after SWE, which occludes LTP between L4-L2/3 synapses in the spared column in vitro (Clem et al., 2008). This difference may be related to the preparations and deprivation time but may also be essential to the difference between the two paradigms. In contrast to SWE (Glazewski et al., 2000), DWE has been shown to cause only minimal expansions of spared whisker representations into deprived columns (Diamond et al., 1994) and thus may be a less-potent driver of LTP than SWE.

Our data imply that a reduced efficacy of SW-associated feedforward inhibition allowed the potentiation of SW-evoked PSPs (Figures 6 and 7). The facilitated STD-LTP may continue to increase surround-evoked excitatory responses and promote connectivity changes in cortical networks (Cheetham et al., 2008; Hardingham et al., 2011; Wilbrecht et al., 2010). The converse may happen during normal experience-dependent development of the barrel cortex. Recent evidence suggests that experience-driven maturation of feedforward inhibitory circuits in L4 is important for the circuit formation and correct sensory processing during postnatal development (Chittajallu and Isaac, 2010). In this case the increased inhibition may tune the strength and timing of PW-related sensory input and decrease the plasticity potential of the SW-related circuit that is also impinging on these cells (Feldman, 2009; Shepherd et al., 2003). In our study the decrease in SW-evoked Gi after DWE was not compensated by a reduction in SW-evoked Ge (Figure 7). This suggests that, differently from complete sensory deprivation (House et al., 2011), partial whisker deprivation disproportionately impacts the SW-associated inhibitory inputs on L2/3 pyramidal cells, not only between spared and deprived barrel columns, but also between two spared barrel columns. This may have been caused by a drop in tonic inhibition (Kelly et al., 1999). This is supported by recent imaging studies in which visual deprivation induced widespread structural remodeling of L2/3 inhibitory cell synapses in the visual cortex (Keck et al., 2011; Chen et al., 2011). Similarly, the removal of a digit in the raccoon is thought to cause disinhibition-driven expansion of cortical receptive fields (Tremere et al., 2001). Conversely, increased sensory stimulation rapidly recruits inhibitory inputs to L4 in the adult barrel cortex, suggesting that inhibition is a tool to reduce receptive field sizes (Knott et al., 2002; Polley et al., 2004). This taken together with our results suggests that cortical disinhibition is a generalized yet crucial event in the early phases of deprivation-mediated cortex plasticity. It is tempting to speculate that whisker-based associative learning-related changes in neighboring column L2/3 cell receptive fields (Rosselet et al., 2011) are also initiated by disinhibition and facilitated STD-LTP.

Could other factors have contributed to the facilitation of STD-LTP in our study? Because whisker deprivation does not alter the NMDAR composition (Clem et al., 2008; Hardingham et al., 2008), it is unlikely that a change in NMDARs has caused the increase in surround STD-LTP in our study. Similar to LTP, surround potentiation in the barrel cortex is dependent on αCamKII autophosphorylation (Glazewski et al., 2000). The addition of synapses could also increase the susceptibility to LTP and thereby contribute to the expansion of barrel cortex receptive fields (Cheetham et al., 2008; Hardingham et al., 2011; Wilbrecht et al., 2010). In addition, deprivation unmasks a PKA-dependent plasticity mechanism that facilitates STD-LTP in deprived barrel columns in vitro (Hardingham et al., 2008), or elicits mGluR-mediated metaplasticity in a singly spared barrel column (Clem et al., 2008). We cannot exclude that such changes in connectivity or postsynaptic molecular machinery contributed to the facilitation of STD-LTP of SW-evoked responses in our study. However, our finding that a GABA-A-R block did not on average enhance the levels of SW-driven STD-LTP after DWE as compared to the nondeprived barrel cortex (Figure 8) strongly suggests that disinhibition was at least an important contributing factor to DWE-mediated STD-LTP facilitation. In conclusion disinhibition-mediated facilitation of STD-LTP is likely to represent a form of metaplasticity that supports the experience-dependent fusion and expansion of receptive fields upon partial sensory deprivation.

EXPERIMENTAL PROCEDURES

Animal Preparation

All procedures were performed according protocols approved by the ethics committee of the University of Geneva and the authorities of the canton of Geneva. Young adult C57Bl/6 male mice (postnatal day [P] 21–P51) were used. Control and deprived (DWE) mice were from the same litters. Experiments on control mice (n = 33; average weight, 13.4 ± 4 g) and deprived mice (n = 28; average weight, 14.1 ± 3 g; p = 0.2) were interleaved. All mice were housed in a moderately enriched environment (some tunnels and climbing racks were provided). For DWE all except the C1 and C2 whiskers on the left side of the snout were trimmed daily under light isoflurane anesthesia to keep the whisker stumps shorter than 2 mm. On the right side of the snout, all whiskers were trimmed. Experiments were performed after 2–4 days of DWE (mean deprivation time, 2.4 ± 0.9 days, n = 28). For control mice all except the C1 and C2 whiskers were trimmed under anesthesia just prior to the experiment. Mice were first anaesthetized with isoflurane (4% for induction with ~0.5 l/min O_2) and then with urethane (1.5 g/kg, i.p., prepared in lactated ringer solution containing 102 mM NaCl, 28 mM Na L-Lactate, 4 mM KCl, 1.5 mM $CaCl_2$). Eye ointment was applied to prevent dehydration. The scalp was locally anesthetized with lidocaine (1%), the periosteum gently removed, and a custom-made plastic chamber was attached to the skull above barrel cortex (centered 1.5 mm posterior from bregma, 3.5–4 mm lateral) with dental acrylic and dental cement. The chamber was filled with sterile cortex buffer (125 mM NaCl, 5 mM KCl, 10 mM glucose, 10 mM HEPES, 2 mM $CaCl_2$, and 2 mM $MgSO_4$ [pH 7.4]) and sealed with a glass coverslip. Intrinsic optical signals (Figures 1A and S1A–S1C) were imaged through the intact skull using an Imager 3001F (Optical Imaging, Mountainside, NJ, USA). For details see Supplemental Experimental Procedures.

After imaging, a small, ~1 × 1 mm piece of bone was removed using a dental drill (centered above the C2 whisker maximum intrinsic optical signal response). The dura was removed, and the craniotomy was covered with agarose (2% in cortex buffer). A glass coverslip was positioned over the agarose (covering more than half of the craniotomy) to reduce heartbeat and breathing-induced motion of the cortex.

In Vivo Whole-Cell Patch Clamp

Whole-cell "blind" patch-clamp recordings were obtained as previously described by Brecht et al. (2003). High-positive pressure (200–300 mbar) was applied to the pipette (5–8 MΩ) to prevent tip occlusion while penetrating the agarose and the pia. After passing the pia the positive pressure was immediately reduced to prevent cortical damage. The pipette was then advanced in 2 μm steps, and pipette resistance was monitored in the conventional voltage-clamp configuration. When the pipette resistance suddenly increased, positive pressure was relieved to obtain a 3–5 gigaohm seal. After break-in, Vm was measured, and dialysis was allowed to occur for at least 5 min before deflecting the whisker. Data were acquired using a Multiclamp 700B Amplifier (Molecular Devices), and digitized at 10 kHz (National Instruments), using MATLAB (MathWorks)-based Ephus software (http://research.janelia.org/labs/display/ephus; The Janelia Farm Research Center). Offline analysis was performed using custom routines written in IGOR Pro (WaveMetrics). All neurons were located between 100 and 275 μm below the pia (Supplemental Experimental Procedures).

Current-clamp recordings were made using a potassium-based internal solution (135 mM potassium gluconate, 4 mM KCl, 10 mM HEPES, 10 mM Na_2-phosphocreatine, 4 mM Mg-ATP, 0.3 mM Na-GTP, 3 mM biocytin, 0.1 mM spermine, pH adjusted to 7.25 with KOH, 285 mOsm). Rs and input resistance (Rin, not including Rs) were monitored with a 100 ms long-lasting hyperpolarizing square pulse 400 ms prior to each whisker deflection, and extracted offline by using a double-exponential fit. Initial Rs and Rin were not different between CTRL and DWE cells (Supplemental Experimental Procedures). Recordings were discarded if one of the following conditions occurred: (1) Vm and Rs exceeded −50mV and 50 MΩ, respectively; (2) spontaneously occurring spikes were not overshooting; and (3) Rs or Rin changed more than 30% over the duration of the experiment. The bridge was usually not balanced, and liquid junction potential was not corrected.

Voltage-clamp recordings were made using a cesium-based internal solution (135 mM caesium methylsulfonate, 4 mM QX-314Cl, 10 mM HEPES, 10 mM Na_2-phosphocreatine, 4 mM Mg-ATP, 0.3 mM Na-GTP, 3 mM biocytin, 0.1 mM spermine, pH adjusted to 7.25 with CsOH, 285 mOsm). Rs and Rin were continuously monitored in response to a −10mV square pulse before each whisker deflection (Figures S4A and S4B; Supplemental Experimental Procedures). Cells were excluded for voltage-clamp analysis if one of the following conditions occurred: (1) Rs became higher than 40 MΩ, (2) Rin/Rs ratio became lower than 3 at break-in or during the experiment, and (3) Rs or Rin changed more than 30% over the duration of the experiment. The whole-cell capacitance and initial Rs were not compensated, but membrane potential was corrected offline for Rs using the equation Vc = Vh − (Rs × Irest), where Vh and Irest correspond to the command holding potential and the resting current at Vh (averaged along a 200-ms-long window before whisker deflection), respectively.

Whisker-Evoked PSP Analysis

Whisker-evoked PSPs were evoked by forth and back deflection of the whisker (100 ms, 0.133 Hz) using piezoelectric ceramic elements attached to a glass pipette ~4 mm away from the skin. The voltage applied to the ceramic was set to evoke a whisker displacement of ~0.6 mm with a ramp of 7–8 ms. The C1 and C2 whiskers were independently deflected by different piezoelectric elements. The amplitudes of the evoked PSPs were more pronounced during down states as opposed to the up states (Figures S1F–S1K). Peak amplitude and integral analysis was performed on each trace and then presented as a mean of at least 30 whisker-evoked responses. To define up and down states, a membrane potential frequency histogram (1mV bin width) was computed for each recorded cell (Figures S1F and S1G). For each trial the average membrane potential was determined (10 ms before the stimulus artifact), and if it overlapped with the potentials of the second peak, the trace was excluded (Figures S1F and S1G). All other PSP analyses were confined to down states. The PSP onset latency was defined as the time point at which the amplitude exceeded 3× SD of the baseline noise over 5 ms prior to stimulation. It was determined based on an average of at least 20 whisker-evoked PSP traces.

STD-LTP Induction

The C1 or C2 whiskers were stimulated every 7.5 s (0.133 Hz) during a baseline period of 5–15 min. For each cell only one of the two whiskers was selected for the pairing with APs. STD-LTP was then induced by pairing each whisker-evoked PSP with a burst of postsynaptic APs (2.7 ± 0.8 [SD] spikes/burst, n = 54) induced by current injection through the patch pipette (500 ± 160 [SD] pA, 50–60 ms, n = 54). Each pairing was repeated every 1.5 s (0.667 Hz) for 178 ± 27 (SD) times (n = 54) over a 3–5 min period (4.4 ± 0.7 [SD] min, n = 54) (Figures S2A–S2C). For each cell the distribution frequency histogram of all evoked spikes was computed, and the mean delay time for the first AP was determined by fitting the first peak with a Gaussian (Figures S2A and S2B). The latter delay was subtracted from the mean onset latency of whisker-evoked PSPs during the baseline period to get the pre-postpairing delay (Figures 2A, S2A, and S2B). DWE did not affect either the passive membrane properties or the excitability of L2/3 pyramidal neurons as revealed by the mean number of APs elicited by increasing current injection (Figures S3A and S3B). After induction of STD-LTP, whisker-evoked PSPs were obtained every 7.5 s for at least 10 min (mean postpairing time: 22 ± 10 min [SD], n = 54). Single trials were not included in the analysis if Rs and Rin changed by more than 30%, and if current-clamp holding potential varied more than 4mV (PW, Vm prepairing, −72.8 ± 3 [SD], Vm postpairing, −73.1 ± 2.5 [SD], n = 11; SW, Vm prepairing, −73.7 ± 4 [SD], Vm postpairing, −74.2 ± 4 [SD], n = 14).

Synaptic Conductance Analysis

Whisker-evoked synaptic conductances were determined using published methods by House et al. (2011) and Monier et al. (2008) in voltage clamp using whisker-induced postsynaptic currents (PSCs) recorded at 5 different holding potentials (Vh = −100, −70, −50, −30, and 0mV; 20 PSCs per Vh; 0.2 Hz). For details and discussion on voltage-clamp recordings and conductance analysis, see Supplemental Experimental Procedures. The onset latencies of

EPSCs and IPSCs were determined at Vh = −100 and 0mV, respectively, similar to the PSP onsets.

Drug Application

GABA-A receptors and NMDARs were blocked by local and intracellular diffusion of PTX (Sigma-Aldrich; 0.1 mM) and the NMDAR open-channel blocker MK-801 (Tocris; 1 mM) in the recording pipette solution, respectively. A total of 0.1 mM of PTX in the pipette permitted similar levels of LTP as could be obtained using 50 μl PTX (50–100 nM) topically applied to the brain but largely avoided epileptic network activity (data not shown).

Statistical Procedures

Data are presented as the mean ± SEM, except where stated differently, e.g., for SD. All statistical tests (MATLAB statistical toolbox; MathWorks) are mentioned in the figure legends. Details of statistical comparisons are provided in the Supplemental Experimental Procedures.

SUPPLEMENTAL INFORMATION

Supplemental Information includes four figures and Supplemental Experimental Procedures and can be found with this article online at http://dx.doi.org/10.1016/j.neuron.2012.05.020.

ACKNOWLEDGMENTS

We thank Daniel Lebrecht and Alan Carleton for help with intrinsic image analysis; and Carl Petersen, Yann Humeau, Alan Carleton, and Egbert Welker for discussions and comments on the manuscript. This work was supported by the Swiss National Science Foundation (Grants 3100AO-120685, CRSI33-127289, and NCCR/SYNAPSY), the International Foundation for Research in Paraplegia (chair Alain Rossier to A.H.), and EMBO (ALTF 226-2010 to F.G.).

Accepted: May 15, 2012
Published: July 26, 2012

REFERENCES

Adesnik, H., and Scanziani, M. (2010). Lateral competition for cortical space by layer-specific horizontal circuits. Nature *464*, 1155–1160.

Armstrong-James, M., Fox, K., and Das-Gupta, A. (1992). Flow of excitation within rat barrel cortex on striking a single vibrissa. J. Neurophysiol. *68*, 1345–1358.

Banerjee, A., Meredith, R.M., Rodríguez-Moreno, A., Mierau, S.B., Auberson, Y.P., and Paulsen, O. (2009). Double dissociation of spike timing-dependent potentiation and depression by subunit-preferring NMDA receptor antagonists in mouse barrel cortex. Cereb. Cortex *19*, 2959–2969.

Brecht, M., Roth, A., and Sakmann, B. (2003). Dynamic receptive fields of reconstructed pyramidal cells in layers 3 and 2 of rat somatosensory barrel cortex. J. Physiol. *553*, 243–265.

Celikel, T., Szostak, V.A., and Feldman, D.E. (2004). Modulation of spike timing by sensory deprivation during induction of cortical map plasticity. Nat. Neurosci. *7*, 534–541.

Cheetham, C.E., Hammond, M.S., McFarlane, R., and Finnerty, G.T. (2008). Altered sensory experience induces targeted rewiring of local excitatory connections in mature neocortex. J. Neurosci. *28*, 9249–9260.

Chen, J.L., Lin, W.C., Cha, J.W., So, P.T., Kubota, Y., and Nedivi, E. (2011). Structural basis for the role of inhibition in facilitating adult brain plasticity. Nat. Neurosci. *14*, 587–594.

Chittajallu, R., and Isaac, J.T. (2010). Emergence of cortical inhibition by coordinated sensory-driven plasticity at distinct synaptic loci. Nat. Neurosci. *13*, 1240–1248.

Clem, R.L., and Barth, A. (2006). Pathway-specific trafficking of native AMPARs by in vivo experience. Neuron *49*, 663–670.

Clem, R.L., Celikel, T., and Barth, A.L. (2008). Ongoing in vivo experience triggers synaptic metaplasticity in the neocortex. Science *319*, 101–104.

Diamond, M.E., Huang, W., and Ebner, F.F. (1994). Laminar comparison of somatosensory cortical plasticity. Science *265*, 1885–1888.

Feldman, D.E. (2000). Timing-based LTP and LTD at vertical inputs to layer II/III pyramidal cells in rat barrel cortex. Neuron *27*, 45–56.

Feldman, D.E. (2009). Synaptic mechanisms for plasticity in neocortex. Annu. Rev. Neurosci. *32*, 33–55.

Finnerty, G.T., Roberts, L.S., and Connors, B.W. (1999). Sensory experience modifies the short-term dynamics of neocortical synapses. Nature *400*, 367–371.

Fox, K., and Wong, R.O. (2005). A comparison of experience-dependent plasticity in the visual and somatosensory systems. Neuron *48*, 465–477.

Froemke, R.C., Poo, M.M., and Dan, Y. (2005). Spike-timing-dependent synaptic plasticity depends on dendritic location. Nature *434*, 221–225.

Froemke, R.C., Merzenich, M.M., and Schreiner, C.E. (2007). A synaptic memory trace for cortical receptive field plasticity. Nature *450*, 425–429.

Glazewski, S., Herman, C., McKenna, M., Chapman, P.F., and Fox, K. (1998). Long-term potentiation in vivo in layers II/III of rat barrel cortex. Neuropharmacology *37*, 581–592.

Glazewski, S., Giese, K.P., Silva, A., and Fox, K. (2000). The role of alpha-CaMKII autophosphorylation in neocortical experience-dependent plasticity. Nat. Neurosci. *3*, 911–918.

Hardingham, N., Glazewski, S., Pakhotin, P., Mizuno, K., Chapman, P.F., Giese, K.P., and Fox, K. (2003). Neocortical long-term potentiation and experience-dependent synaptic plasticity require alpha-calcium/calmodulin-dependent protein kinase II autophosphorylation. J. Neurosci. *23*, 4428–4436.

Hardingham, N., Wright, N., Dachtler, J., and Fox, K. (2008). Sensory deprivation unmasks a PKA-dependent synaptic plasticity mechanism that operates in parallel with CaMKII. Neuron *60*, 861–874.

Hardingham, N.R., Gould, T., and Fox, K. (2011). Anatomical and sensory experiential determinants of synaptic plasticity in layer 2/3 pyramidal neurons of mouse barrel cortex. J. Comp. Neurol. *519*, 2090–2124.

House, D.R., Elstrott, J., Koh, E., Chung, J., and Feldman, D.E. (2011). Parallel regulation of feedforward inhibition and excitation during whisker map plasticity. Neuron *72*, 819–831.

Humeau, Y., Herry, C., Kemp, N., Shaban, H., Fourcaudot, E., Bissière, S., and Lüthi, A. (2005). Dendritic spine heterogeneity determines afferent-specific Hebbian plasticity in the amygdala. Neuron *45*, 119–131.

Jacob, V., Brasier, D.J., Erchova, I., Feldman, D., and Shulz, D.E. (2007). Spike timing-dependent synaptic depression in the in vivo barrel cortex of the rat. J. Neurosci. *27*, 1271–1284.

Jiao, Y., Zhang, C., Yanagawa, Y., and Sun, Q.Q. (2006). Major effects of sensory experiences on the neocortical inhibitory circuits. J. Neurosci. *26*, 8691–8701.

Keck, T., Scheuss, V., Jacobsen, R.I., Wierenga, C.J., Eysel, U.T., Bonhoeffer, T., and Hübener, M. (2011). Loss of sensory input causes rapid structural changes of inhibitory neurons in adult mouse visual cortex. Neuron *71*, 869–882.

Kelly, M.K., Carvell, G.E., Kodger, J.M., and Simons, D.J. (1999). Sensory loss by selected whisker removal produces immediate disinhibition in the somatosensory cortex of behaving rats. J. Neurosci. *19*, 9117–9125.

Kimura, F., Itami, C., Ikezoe, K., Tamura, H., Fujita, I., Yanagawa, Y., Obata, K., and Ohshima, M. (2010). Fast activation of feedforward inhibitory neurons from thalamic input and its relevance to the regulation of spike sequences in the barrel cortex. J. Physiol. *588*, 2769–2787.

Knott, G.W., Quairiaux, C., Genoud, C., and Welker, E. (2002). Formation of dendritic spines with GABAergic synapses induced by whisker stimulation in adult mice. Neuron *34*, 265–273.

Komai, S., Licznerski, P., Cetin, A., Waters, J., Denk, W., Brecht, M., and Osten, P. (2006). Postsynaptic excitability is necessary for strengthening of cortical sensory responses during experience-dependent development. Nat. Neurosci. *9*, 1125–1133.

Li, C.X., Callaway, J.C., and Waters, R.S. (2002). Removal of GABAergic inhibition alters subthreshold input in neurons in forepaw barrel subfield (FBS) in rat first somatosensory cortex (SI) after digit stimulation. Exp. Brain Res. *145*, 411–428.

Lübke, J., and Feldmeyer, D. (2007). Excitatory signal flow and connectivity in a cortical column: focus on barrel cortex. Brain Struct. Funct. *212*, 3–17.

Manookin, M.B., Beaudoin, D.L., Ernst, Z.R., Flagel, L.J., and Demb, J.B. (2008). Disinhibition combines with excitation to extend the operating range of the OFF visual pathway in daylight. J. Neurosci. *28*, 4136–4150.

Markram, H., Lübke, J., Frotscher, M., and Sakmann, B. (1997). Regulation of synaptic efficacy by coincidence of postsynaptic APs and EPSPs. Science *275*, 213–215.

Meliza, C.D., and Dan, Y. (2006). Receptive-field modification in rat visual cortex induced by paired visual stimulation and single-cell spiking. Neuron *49*, 183–189.

Merzenich, M.M., Kaas, J.H., Wall, J., Nelson, R.J., Sur, M., and Felleman, D. (1983). Topographic reorganization of somatosensory cortical areas 3b and 1 in adult monkeys following restricted deafferentation. Neuroscience *8*, 33–55.

Micheva, K.D., and Beaulieu, C. (1995). An anatomical substrate for experience-dependent plasticity of the rat barrel field cortex. Proc. Natl. Acad. Sci. USA *92*, 11834–11838.

Monier, C., Fournier, J., and Frégnac, Y. (2008). In vitro and in vivo measures of evoked excitatory and inhibitory conductance dynamics in sensory cortices. J. Neurosci. Methods *169*, 323–365.

Petersen, C.C., Grinvald, A., and Sakmann, B. (2003). Spatiotemporal dynamics of sensory responses in layer 2/3 of rat barrel cortex measured in vivo by voltage-sensitive dye imaging combined with whole-cell voltage recordings and neuron reconstructions. J. Neurosci. *23*, 1298–1309.

Petreanu, L., Mao, T., Sternson, S.M., and Svoboda, K. (2009). The subcellular organization of neocortical excitatory connections. Nature *457*, 1142–1145.

Polley, D.B., Kvasnák, E., and Frostig, R.D. (2004). Naturalistic experience transforms sensory maps in the adult cortex of caged animals. Nature *429*, 67–71.

Pouille, F., and Scanziani, M. (2001). Enforcement of temporal fidelity in pyramidal cells by somatic feed-forward inhibition. Science *293*, 1159–1163.

Rosselet, C., Fieschi, M., Hugues, S., and Bureau, I. (2011). Associative learning changes the organization of functional excitatory circuits targeting the supragranular layers of mouse barrel cortex. Front. Neural Circuits *4*, 126.

Sato, T.R., Gray, N.W., Mainen, Z.F., and Svoboda, K. (2007). The functional microarchitecture of the mouse barrel cortex. PLoS Biol. *5*, e189.

Shepherd, G.M., Pologruto, T.A., and Svoboda, K. (2003). Circuit analysis of experience-dependent plasticity in the developing rat barrel cortex. Neuron *38*, 277–289.

Sjöström, P.J., Rancz, E.A., Roth, A., and Häusser, M. (2008). Dendritic excitability and synaptic plasticity. Physiol. Rev. *88*, 769–840.

Swadlow, H.A., and Gusev, A.G. (2002). Receptive-field construction in cortical inhibitory interneurons. Nat. Neurosci. *5*, 403–404.

Takahashi, T., Svoboda, K., and Malinow, R. (2003). Experience strengthening transmission by driving AMPA receptors into synapses. Science *299*, 1585–1588.

Tremere, L., Hicks, T.P., and Rasmusson, D.D. (2001). Role of inhibition in cortical reorganization of the adult raccoon revealed by microiontophoretic blockade of GABA(A) receptors. J. Neurophysiol. *86*, 94–103.

Tsubokawa, H., and Ross, W.N. (1996). IPSPs modulate spike backpropagation and associated [Ca2+]i changes in the dendrites of hippocampal CA1 pyramidal neurons. J. Neurophysiol. *76*, 2896–2906.

Van der Loos, H., and Woolsey, T.A. (1973). Somatosensory cortex: structural alterations following early injury to sense organs. Science *179*, 395–398.

Varga, Z., Jia, H., Sakmann, B., and Konnerth, A. (2011). Dendritic coding of multiple sensory inputs in single cortical neurons in vivo. Proc. Natl. Acad. Sci. USA *108*, 15420–15425.

Wilbrecht, L., Holtmaat, A., Wright, N., Fox, K., and Svoboda, K. (2010). Structural plasticity underlies experience-dependent functional plasticity of cortical circuits. J. Neurosci. *30*, 4927–4932.

Wilent, W.B., and Contreras, D. (2004). Synaptic responses to whisker deflections in rat barrel cortex as a function of cortical layer and stimulus intensity. J. Neurosci. *24*, 3985–3998.

Young, J.M., Waleszczyk, W.J., Wang, C., Calford, M.B., Dreher, B., and Obermayer, K. (2007). Cortical reorganization consistent with spike timing-but not correlation-dependent plasticity. Nat. Neurosci. *10*, 887–895.